Peer-reviewed version available at J. Imaging 2018, 4, 42; doi:10.3390/jimaging4020042

Article

Analytical study of colour spaces for plant pixel detection

Pankaj Kumar [1,‡], and Stanley J. Miklavcic [2,‡]

‡ School of Information Technology and Mathematical Sciences;
Phenomics and Bioinformatics Research Centre
University of South Australia
Mawson Lakes, SA 5095
1 pankaj.kumar@unisa.edu.au
2 stan.miklavcic@unisa.edu.au
* Correspondence: pankaj.kumar@unisa.edu.au; Tel.: +61-8-830-23196
‡ These authors contributed equally to this work.

Abstract: Segmentation of a region of interest is an important pre-processing step for many colour image analysis techniques. Similarly segmentation of plant in digital images is an important preprocessing step in phenotying plants by image analysis. In this paper we present an analytical study to statistically determine the suitability of colour space representation of an image to best detect plant pixels and separate them from background pixels. Our hypothesis is that the colour space representation in which the separation of the distributions representing plant pixels and background pixels is maximized would be the best for detection of plant pixels. The two classes of pixels are modelled as a Gaussian mixture model (GMM). In our GM modelling we don't make any prior assumption about the number of Gaussians in the model. Rather a constant bandwidth mean-shift filter is used to cluster the data and the number of clusters and hence the number of Gaussians is automatically determined. Here we have analysed following representative colour spaces like RGB, rgb, HSV, $Ycbcr$ and $CIE-Lab$. This is because these colour spaces represent several other similar colour spaces and also an exhaustive study of all the colour space will be too voluminous. We also analyse the colour space feature from the two-class variance ratio perspective and compare the results of our hypothesis with this metric. The dataset for this empirical study consist of 378 digital images of plants and their manual segmentation. Dataset consist of various species of plants (arabidopsi, tobacco, wheat, rye grass etc.) imaged under different lighting conditions, indoor and outdoor, controlled and uncontrolled background. In results we obtain better segmentation of the plants in HSV colour space, which is supported by its Earth mover distance (EMD) on the GMM distribution of plant and background pixels.

Keywords: Plant phenotyping, Plant pixel classification, Colour space, , Gaussian mixture model, Earth mover distance, Variance ratio, Plant segmentation.

1. Introduction

Compared with the growing interest in plant phenotyping using computer vision and image analysis, plant phenotyping by visual inspection is slow and subjective relying as it does on human evaluation. Two of the aims of digital imaging and image analysis are to remove any degree of subjectivity associated with an individual human's perception and to expedite the procedure. This is especially relevant for high throughput assessment of genetic expression which is manifested in the variation of phenotypic traits in plants.

Another and particular application of digital imaging in an agricultural setting is the detection and identification of weeds for the purpose of spot spraying of herbicide. Spot spraying, as opposed to blanket spraying, is more economical and environmentally less detrimental. It bears considering that successful application of spot spraying may also depend on weed size (volume of herbicide) as well as

weed identification (type of herbicide). Consequently, being able to estimate weed volume or biomass by 3D reconstruction from digital images is potentially beneficial. In [1] An *et. al.* presented a novel method that used plant segmentation from plant images for 3D plant morphology quantification and phenotyping. Plant segmentation was used by An *et. al.* in [2] to measure phenotypic traits such as leaf length and rosette area in 2D images. Plant pixel detection by a GMM was used by Natalia *et. al.* in [3] for automatic detection of plot canopy coverage and analysing different genotypes based on this observation. Thus it can be noted that an important basic precursor to both detection, identification and 3D reconstruction [4,5] is the process of segmenting plant objects from their background in an image. That is, the detection of plant pixels by the binary classification of pixels into plant or non-plant groups.

There are many approaches to segmentation. These can fall into one of two camps: supervised or unsupervised segmentation [4,6]. However, active contours or level sets and fuzzy logic can also be used for object segmentation [7,8]. All these different methods of segmentation will benefit from the study presented in this paper. A colour space which improves the separability of plant pixels and not plant pixels will all the above methods in performing better segmentation of plant regions.

Many segmentation methods are based on color distinction. To achieve optimal plant segmentation, however, the question naturally arises of which colour space is the more effective for the detection of plant pixels? Is there a suitable transformation of {Red Green Blue} (RGB)colour space to a representation that will make plant pixel detection more accurate and more reliable? Can a suitable representation be found that will improve the degree to which plant pixel detection is invariant to illumination condition? Does the contrast between plants and background naturally get enhanced in certain colour space irrespective of the illumination conditions? These are some of the questions we address in this paper. Similar questions have been raised and answered for skin pixel segmentation [9–11], shadow and traffic object detection [12–14] and image segmentation by graph cut in [15,16]. Choice of color spaces influences object recognition see [17] for more details.

A related study seeking to improve plant segmentation by colour analysis was carried out by Golzarian *et al.* [18] using colour indices. Colour indices, individually, however, do not provide a complete representation of a colour space, as individual indices are scalar-valued variables obtained by a linear manipulation of the components of the three dimensional colour space vector variable for a pixel. The individual colour indices considered by Golzarian *et al.* [18] were g, DGR, EGI, $MEGI$, NDI, and Hue, the hue channel of HSV colour space. Their results showed that hue achieved the least amount of type II error with a small loss of plant pixel. Our results and conclusions differ, however, an outcome which we attribute to the fact that our study is more encompassing as our larger dataset includes a greater number of lighting conditions and a larger number of plant species. Thus, in contrast to Golzarian *et al.*'s findings, our results show that HSV is overall best suited for segmentation of plants under the majority of lighting conditions.

This paper is organized as follows. In Section 2.1 we introduce briefly the different colour spaces we experimented with and their mathematical relationship to each other. Then, in Section 2.2 we outline our method for discriminating pixels into one of two classes using on Gaussian Mixture Models (GMMs) and evaluating the separability of the classes by computing the class distance using earth mover distance (EMD) and variance ratios. EMD [19] has a long history for use in image processing and analysis. Rubner *et. al.* used EMD on cluster signature of images for image retrieval and for object tracking by Zhao *et al.* in [20] and by Kumar *et al.* in [21]. The details of our dataset are provided in 2. We present our results and discuss those in Section 3, and finally conclude the paper with summary comments in Section 4.

2. Methods

2.1. Colour Representation

Colour spaces allow for different representations of intensity and colour information in colour images. Past research activities on colour representation, psychovisual perception of colour, video signal transmission and computer graphics have given rise to many colour spaces with different desirable properties. Here, we briefly review the colour spaces that we shall utilize and summarize how they are related to the common RGB colour space.

2.1.1. RGB

Red, green, and blue are the familiar primary colours and it is now accepted that their different practical combinations are capable of generating almost all possible colour shades. This colour space has been the basis for the design of CRTs, television and computer screens. Most still cameras and scanners save their images in this colour space. However, the high correlation between channels as well as the mixing of chrominance and luminance information makes RGB space an unfavourable choice for colour-based detection schemes.

2.1.2. Normalized rgb

$$r = \frac{R}{R+G+B}, \quad g = \frac{G}{R+G+B}, \quad b = \frac{B}{R+G+B} \tag{1}$$

This is a colour space in which intensity information is normalized, which in turn leads to a reduced dependence on the luminance information. The normalization property, however, makes on the three components redundant. For instance, no additional information is available in b since $b = 1 - r - g$. In such a case, the components, r and g, are referred to as pure colours due to the absence of a dependence on the brightness of the source RGB.

2.1.3. HSV

This colour space specifies any colour in terms of three quantities: Hue, Saturation, and Value. It was introduced to satisfy user need to specify colour properties numerically. Hue defines the dominant colour of a pixel, Saturation measures the colourfulness of a pixel in proportion to its brightness and Value is related to the colour luminance. HSV is non-linearly related to RGB via the following set of equations

$$\begin{aligned} H &= \begin{cases} \theta & \text{if } B \le G, \\ 360^\circ - \theta & \text{if } B > G. \end{cases} \\ &\quad \text{where} \quad \theta = cos^{-1} \frac{1/2[(R-G)+(R-B)]}{[(R-G)^2+(R-B)(G-B)]^{1/2}} \\ S &= 1 - \frac{3}{R+G+B}[min(R,G,B)] \\ V &= 1/3(R+G+B) \end{aligned} \tag{2}$$

A polar co-ordinate representation of HSV results in a cyclic colour space. This colour space is similar to the colour space representations, HIS, HLS, and HCI.

2.1.4. $Ycbcr$

This colour space is utilized in most image compression standards such as $JPEG$, $H.261$, $MPEG$, and television studios (video cameras also usually save in this format). Pixel intensity is represented by Y luminance, computed as the weighted sum of RGB values, the weight matrix which transforms the

RGB pixel value to $Ycbcr$ is given in equation 3. The chrominance component of the pixel information is contained in the cb and cr channels. The colour space is characterized by a simple but explicit separation of luminance and chrominance components. It is similar to YIQ and YUV color spaces and linearly related to RGB as follows

$$\begin{bmatrix} Y \\ cr \\ cb \end{bmatrix} = \begin{bmatrix} 0.299 & 0.587 & 0.114 \\ 0.711 & -0.587 & -0.114 \\ -0.299 & -0.587 & 0.886 \end{bmatrix} \times \begin{bmatrix} R \\ G \\ B \end{bmatrix} \tag{3}$$

where the matrix elements are fixed.

2.1.5. CIE-Lab

This colour space, originally proposed by G. Wyszecki [22], to approximate perceptually-uniform colour space information has been standardized by the Commission Internationale de L' Eclairage (CIE). By "perceptually-uniform" one means that it was designed to approximate human vision. The $L-$channel contains information about pixel intensity/brightness, where as a and b stores the colour information. The $CIE-Lab$ colour space is non-linearly related to $CIE-XYZ$ The RGB to XYZ conversion is achieved by a linear transformation involving a matrix, $\mathbf{M}$: $\begin{bmatrix} X \\ Y \\ Z \end{bmatrix} = \mathbf{M} \begin{bmatrix} R \\ G \\ B \end{bmatrix}$. There is a standard method of computing $\mathbf{M}$ when the co-ordinates of the RGB system and reference white has been specified. One such $\mathbf{M}$ has been used in [14] for $sRGB$, $D65$ device-dependent colour space. Related colour spaces are $CIE-LUV$ and $CIE-LCH$. More details of the different colour spaces could be found in [23].

2.2. Evaluation of colour space representations

To evaluate the suitability of a colour space representation for the detection of plant pixels, we differentiate background from foreground pixels based on their relative position within a Gaussian Mixture Model (GMM) which has been constructed using the respective colour space information possess by the pixels. The Gaussian Mixture Model is a function of a random variable, $\mathbf{z}$, which in our case is the feature vector comprising the information in the three pixel colour channels:

$$gmm(\mathbf{z}, \boldsymbol{\phi}) = \sum_{k=1}^{K} w_k g(\mathbf{z} : \boldsymbol{\mu}_k, \boldsymbol{\Sigma}_k) \tag{4}$$

The model parameter set $\boldsymbol{\phi}$ is the set $\{w_k, \boldsymbol{\mu}_k, \boldsymbol{\Sigma}_k\}_{k=1}^{K}$ where K is the number of Gaussian distributions in gmm and each g is of the form

$$g(\mathbf{z} : \boldsymbol{\mu}_k, \boldsymbol{\Sigma}_k) = \frac{1}{\sqrt{2\pi}\boldsymbol{\Sigma}_k} e^{\frac{-1}{2}(\frac{\|\mathbf{z}-\boldsymbol{\mu}_k\|}{\boldsymbol{\Sigma}_k})^2}. \tag{5}$$

In applying the GMM using the expectation maximization (EM) algorithm, there arises the fundamental problem of how to predetermine the number of Gaussian functions to include in the GMM. We ameliorate this problem by using a mean-shift algorithm to cluster both the background pixel and foreground plant pixel data. The same fixed bandwidth is used to cluster both sets of pixel data. Each cluster is then modelled as a Gaussian distribution with a diagonal co-variance matrix,

$$\boldsymbol{\Sigma}_k = \begin{bmatrix} \sigma_{11} & 0 & 0 \\ 0 & \sigma_{22} & 0 \\ 0 & 0 & \sigma_{33} \end{bmatrix}. \tag{6}$$

This is utilized to reduce computational load at the cost of an insignificant loss of accuracy. We denote the background GMM be gmm_{bg} and foreground plant pixel GMM be gmm_{fg}. A distance function based on Earth Mover Distance (EMD) is used as a measure of the distance between gmm_{bg} and gmm_{fg}. The EMD can be considered as a measure of dissimilarity between two multi-dimensional distributions. The greater the EMD between two distributions the more dissimilar they are. It was used by Rubner *et al.* in [24] for colour- and texture-based image retrieval. It was also employed by Kumar and Dick in [21] to track targets in an image sequence. In the present case we apply the EMD measure to the multi-dimensional Gaussian mixture distributions that correspond, respectively, to background and foreground/plant pixel colour in a given colour space. We then consider the relative success of the EMD-based clustering in the different colour spaces to compare the effectiveness of the spaces. The greater the EMD value between the background and foreground GMMs in a different colour spaces, the better is that colour space for separating plant pixel from non-plant pixel. Using an EMD as a quantifier we aim to discover in which colour space the distance between the two distributions is maximal. We will then explore how this distance varies with changes in plant type and imaging conditions.

Computing the EMD is based on a solution of the transportation problem [25]. For our situation the two distributions are the GMMs corresponding to the two classes of plant pixel and background pixel:

$$\begin{aligned} gmm_{bg} &= \sum_{l=1}^{L} w_l g(\mathbf{z} : \boldsymbol{\mu}_l, \boldsymbol{\Sigma}_l) \quad and \\ gmm_{fg} &= \sum_{k=1}^{K} w_k g(\mathbf{z} : \boldsymbol{\mu}_k, \boldsymbol{\Sigma}_k). \end{aligned} \tag{7}$$

Here, gmm_{bg} has L Gaussians in its model and gmm_{fg}has t). To compute the EMD between them. L need not be equal to K.

2.2.1. EMD on GMMs

Here we provide an overview for the use of EMD as a measure of separation/distance between two Gaussian mixture model (GMM) distributions. Let the two distributions, gmm_{bg} and gmm_{fg}, be characterized by their weights, means, and variances, $(w_l, \boldsymbol{\mu}_l, \boldsymbol{\Sigma}_l)_{l=1}^{L}$ and $(w_k, \boldsymbol{\mu}_k, \boldsymbol{\Sigma}_k)_{k=1}^{K}$. The EMD is used to compute the distance between these cluster signatures. Cluster signatures are characterised by weights; a signature differs from a distribution in the sense that the weights are not normalized. Also, cluster signatures do not have a cluster spread associated with them as the GMMs have variances associated with each Gaussian. In our case the weights $w_k\{k = 1...K\}$ are normalized, *i.e.*, $\sum_{k=1}^{K} w_k = 1$. EMD can also be used for computing the dissimilarity between unnormalized cluster signatures. However, in our application the weights are normalized. The EMD is defined in terms of an optimal flow f_{kl} which minimizes the following

$$EMD(gmm_{fg}, gmm_{bg}) = \sum_{k=1}^{K} \sum_{l=1}^{L} f_{kl} d_{kl}, \tag{8}$$

where $d_{lk} = D(g(\mathbf{z} : \boldsymbol{\mu}_k, \boldsymbol{\Sigma}_k), g(\mathbf{z} : \boldsymbol{\mu}_l, \boldsymbol{\Sigma}_l))$ is a measure of dissimilarity/distance between $g(\mathbf{z} : \boldsymbol{\mu}_k, \boldsymbol{\Sigma}_k)$ and $g(\mathbf{z} : \boldsymbol{\mu}_l, \boldsymbol{\Sigma}_l)$ and is also referred to as ground distance (GD). The computed flow after an optimization process satisfies the following constraints

$$\begin{aligned} f_{kl} &\geq 0, \quad for\ 1 \leq l \leq L,\ 1 \leq k \leq K \\ \sum_{l=1}^{L} f_{kl} &\leq w_k, \quad for\ 1 \leq k \leq K \\ \sum_{k=1}^{K} f_{kl} &\leq w_l, \quad for\ 1 \leq l \leq L \\ \sum_{k=1}^{K}\sum_{l=1}^{L} f_{kl} &= min(\sum_{k=1}^{K} w_k, \sum_{l=1}^{L} w_l) = 1 \end{aligned} \tag{9}$$

The formulation of EMD is slightly different when the weights are not normalized. We have used the C code provided by Rubner *et. al* for computation of EMD, implemented according to their paper [26]. A Matlab wrapper over the C code was implemented for data exchange and calling of the C function from a matlab script. The code for EMD computation was optimized by use of an efficient algorithm for the transportation problem. There are many more efficient implementations of EMD such as [27,28]. In [28] the authors made improvements to the efficiency by assuming that EMD was used to compare histograms. However here we compared distributions that were modelled using the GMM. In [27] the authors computed approximate EMD in linear time. We decided not to use an approximate computation of EMD for our experiments. Furthermore, the number of Gaussians in the GMM representation of data was of the order of 10. Hence speed of EMD computation never became a bottle neck in our experiments. For computing the ground distance d_{lk} we need a distance measure between two Gaussians $g(\mathbf{z} : \boldsymbol{\mu}_l, \boldsymbol{\Sigma}_l)$ and $g(\mathbf{z} : \boldsymbol{\mu}_k, \boldsymbol{\Sigma}_k)$. We propose here to use a modified Mahalanobis distance to compute the ground distance d_{lk} between two Gaussians l, k

$$d_{lk} = (\boldsymbol{\mu}_l - \boldsymbol{\mu}_k)^T[(\boldsymbol{\Sigma}_l + \boldsymbol{\Sigma}_k)/2]^{-1}(\boldsymbol{\mu}_l - \boldsymbol{\mu}_k). \tag{10}$$

The Mahalanobis distance, formally introduced by P.C. Mahalanobis in [29], is a measure of similarity/difference of a multivariate data point $\mathbf{z} = (z_1, z_2, ..., z_N)$ with a known Gaussian distribution in the same dimension

$$D_M(\mathbf{z}) = \sqrt{(\mathbf{z} - \boldsymbol{\mu})^T \boldsymbol{\Sigma}^{-1} (\mathbf{z} - \boldsymbol{\mu})} \tag{11}$$

This distance is different from Euclidean distance in that it scales down the distance by the standard deviation of the distribution. The intuition behind this distance is that distance of a data point from a normal distribution is inversely proportional to its spread. This is an important concept in cluster analysis. The distance of a data point to a cluster is not just the Euclidean distance of the data point to the cluster centre. It also depends inversely on the spread of the cluster. The same intuitive notion extends to the distance between two Gaussians, as suggested by the distance function in equation (10). The distance between two Gaussians with similar differences in means increases as their standard deviation decreases. A problem with the distance function in equation (10) is that it becomes unbounded as the variance of the Gaussian goes to zero. However, this phenomena is of theoretical interest only, as in real life data sets it is seldom possible to model something with zero variance normal distribution. Furthermore, a zero variance normal distribution has no physical meaning. Other distance functions like Bhattacharyya distance, Hellinger distance, Kulback Leibler etc., could also have been modified to formulate a distance function between two multivariate Gaussian and in future studies we will consider this aspect of the problem.

2.2.2. Two class variance ratio

To study the discriminative power of different colour spaces with respect to segmenting plant pixels from background pixels, we compare the results of the present approach to results of augmented

variance ratio (AVR). AVR has been used for feature ranking and as a preprocessing step in feature subset selection [30,31], and for online selection of discriminative feature tracking [32]. AVR is defined as the ratio of the inter-class variance to the intra-class variance of features. We use this variance ratio to measure the power of different colour spaces to discriminate plant pixel from background pixel. It is well known that linear discriminant analysis (LDA) and the variance ratio are inappropriate for separating multi-modal class distributions. The plant pixel colours and background pixel colours are generally multi-model. Therefore, we use the log-likelihood ratio, a non-linear transformation, to transform the features of a pixel i

$$L(i) = log\frac{max(pp(i),\delta)}{max(bg(i),\delta)} \tag{12}$$

The parameter δ is set to a small value, *e.g.*, 0.001, to avoid creating a divergence (divide by zero or logarithm of zero). The vectors $pp(i)$ and $bg(i)$ are the class conditional probability distributions (normalized histogram) of plant and background pixels, respectively, learnt from a training data set. This log likelihood makes the class distributions more uni-modal making the use of variance ratio appropriate for measuring the discriminative power of the colour space feature. The variance of $L(i)$ for class $pp(i)$ is

$$\begin{aligned} var(L;pp) &= E[L^2(i)] - (E[L(i)])^2 \\ &= \sum_i pp(i)L^2(i) - [\sum_i pp(i)L(i)]^2 \end{aligned} \tag{13}$$

Similarly variance ratio for background class is

$$var(L;bg) = \sum_i bg(i)L^2(i) - [\sum_i bg(i)L(i)]^2 \tag{14}$$

The variance ratio now is

$$VR(L;pp,bg) = \frac{var(L;(pp+bg)/2)}{var(L;pp)+var(L;bg)} \tag{15}$$

The denominator ensures that colour space in which within class variance is smaller will be more discriminative and the numerator favours the feature space in which between class variance is larger.

2.3. Dataset and Experiments

The data set contains images under controlled lighting conditions of Arabidopsis and tobacco plants grown in growth chambers. A distinct part of the data set consists of wheat and rye grass images, which have been taken under different lighting conditions in the field and different types of soils and mulch. Figure 1 shows the two imaging platforms used for imaging some of the plants used in this study. The platform on the left is for imaging indoor plants and platform on the right is for imaging outdoor plants. After imaging the plant region was manually selected and segmented for this study. Arabidopsis images have two types of backgrounds: one black, the other red. Plants used in this study were imaged both indoors and outdoors, as we are trying to capture lot of varieties in the illumination conditions. Figure 2 show some sample images from our dataset used in this study and their manual segmentation.

For segmentation of images in different colour spaces we used mean-shift clustering and region fusion. We then selected the cluster related to leaves in a semi-supervised way. We did a two pass mean-shift clustering. The first pass was to determine the leaf area and separate it from the background. The second pass was to cluster individual leaves and separate them into different leaf areas. Different sets of parameters where used for the two passes of the clustering algorithm as given in [6].

Peer-reviewed version available at J. Imaging 2018, 4, 42; doi:10.3390/jimaging4020042

(a) (b)

Figure 1. This figure shows the two imaging platforms we have build in house for imaging plants. (a) is the platform for imaging plants indoor and (b) is the platform for imaging outdoor plants growing in field condition.

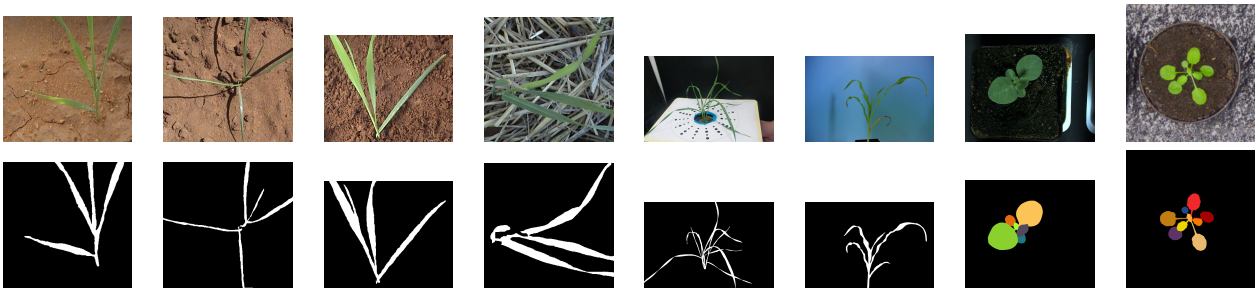

Figure 2. This figure shows some sample images and their manual segmentation and labelling from the data set used in this study

Peer-reviewed version available at J. Imaging 2018, 4, 42; doi:10.3390/jimaging4020042

Table 1. Table for different plant types and the computed EMD on the GMM models in different colour spaces and their comparison with variance ratio in different colour spaces. EMD based distance are higher for HSV on both plant types, where as variance ratios are higher for normalized rgb colour space.

Plant type	Colour Space	EMD distance	Variance ratio
Arabidopsis	RGB	282.46	1.17
	HSV	**847.24**	1.09
	$CIE-Lab$	246.14	2.19
	$nrgb$	264.66	**2.23**
	$YCbCr$	155.01	1.67
Tobacco	RGB	228.65	0.76
	HSV	**1389.56**	0.99
	$CIE-Lab$	415.17	0.43
	$nrgb$	347.63	**1.11**
	$YCbCr$	235.15	0.47

Table 2. Table for different imaging senarios for same plant type. Their computed EMDs on the GMM models in different colour spaces and their comparsion with variance ratio in different colour spaces. EMD based distance are higher for HSV on both background types, where as variance ratios are higher for normalized rgb colour space for contrasting red background and $CIE-Lab$ for the black background.

Background type	Colour Space	EMD distance	Variance ratio
Contrasting Green-Red	RGB	230.36	1.06
	HSV	**401.81**	0.78
	$CIE-Lab$	182.77	1.77
	$nrgb$	39.43	**1.88**
	$YCbCr$	178.47	1.57
Green-Black	RGB	282.16	1.27
	HSV	**404.70**	2.13
	$CIE-Lab$	272.88	**9.17**
	$nrgb$	257.87	2.24
	$YCbCr$	181.57	3.62

3. Results

The results of applying the proposed EMD measure, Eq (8), on the GMMs of foreground and background pixels from training data are shown in Tables 1 and 2. These tables also show the variance ratios given by Eq (15) for the two classes of pixels in different colour channels. The HSV colour space seems to be the highest scoring of all systems in terms of EMD distance over the GMMs of plant pixels and background pixels. There is no clear uniformally high performance achiever amongst the different colour spaces, in terms of the variance ratios. The segmentation results shown in Figure 3 and in Table 3, show that segmentation based on the HSV colour space is superior in two out of three different scenarios. Table 3 shows segmentation in terms of percentages using the FGBGDice code provided by the LSC challange dataset. Finally, we show the segmentation results for the test data set in $CIE-Lab$ colour space. The reason for using the $CIE-Lab$ colour space for this comparison is that this colour space was recommended by the authors of [6].

The segmentation results for separating plant leaves from the background obtained on the test data for Arabidopsis were quite reasonable, achieving mean values of 0.9215 with a standard deviation of 0.0282 on A1 test images (see Table 4) and a mean of 0.93313 with a standard deviation of 0.0241 for test images of A2 (see Table 4). Set A1 are Arabidopsis plants with red background imaged indoor under controlled lighting condition and A2 are different Arabidopsis plants with black background also imaged indoor. Set A3 are the tobacoo plants under different stages of development. Some errors in plant and background segmentation were mainly due to the presence of green moss on the

Peer-reviewed version available at J. Imaging 2018, 4, 42; doi:10.3390/jimaging4020042

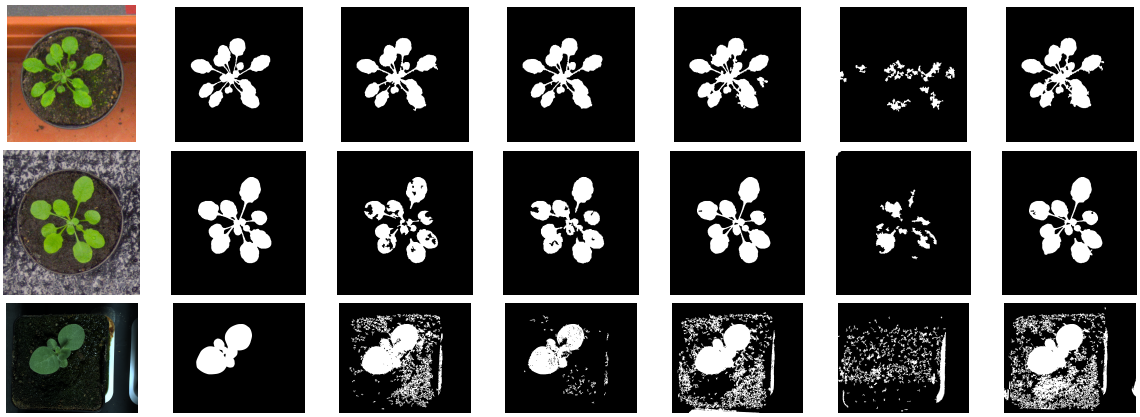

Figure 3. This figure shows the results of segmentation using the method of mean-shit clustering, used in the paper, for different colour spaces. Image in column (a) are the original images of Arabidopsis and Tobacco plants. One set of Arabidopsis plant has a contrasting red background and the other has black background. The images in column (b) are the ground truth segmentation results. The ground truth segmentation were generated by manual labelling of the image data. In columns (c), (d), (e), (f), and (g) are the segmentation in different colour spaces RGB, HSV, $CIE-Lab$, normalized rgb, and $YCbCr$, respectively

Table 3. Percentage foreground background segmentation results in the different colour spaces for there different datasets. A1's are Arabidopsis plants with a red background, A2's are Arabidopsis plants with black background and A3's are tobacoo plants imaged in controlled growth chambers.

Plant type	P ercentage Foreground Background Segmentation				
	RGB	HSV	$CIE-Lab$	rgb	$YCbCr$
A1	96.32 %	96.67%	93.40%	10.87%	94.25%
A2	90.53%	95.54%	98.51%	49.69%	97.83%
A3	64.8%	89.6%	57.23%	19.56%	51.79%

Table 4. Overall plant and leaf segmention results using the method of mean-shift clustering as described in Section 2

Plant type	P lant segmentation		L eaf Segmentation	
	Mean	Std	Mean	Std
A1	92.14%	2.82 %	47.14%	11.14%
A2	93.31%	2.41 %	55.16%	13.15%
A3	76.52%	35.32%	34.03%	22.35%

background soil. The leaf segmentation results were not as good as the plant segmentation results because the algorithm was designed mainly for background-foreground segmentation. The results can be improved with the use of shape prior for leaf segmentation. The accuracy of plant segmentation for the tobacco test data set was quite poor. We speculate that this result can be attributed to two reasons. Firstly, the colours of some of the tobacco plant leaves in the test data set were quite different from what was typically found in the training data set. Secondly, the illumination present in the tobacco images was not as intense as that present in the Arabidopsis plant images. Consequently, some of the darker regions of the tobacco plants were classified as background.

Plant pixel detection and segmentation is certainly affected by the choice of the colour space being used for image analysis. Hence it should be carefully considered which colour space to use for plant phenotyping by digital image analysis. In this study where we considered and analysed five different colour spaces, better plant pixel detection was achieved in HSV colour space for almost all plant types and under different illumination conditions. This can be attributed to the fact that HSV is a perceptual colour space. Usually better results of detection and segmentation are obtained in perceptual colour spaces. This observation of ours is supported by Golzarian *et. al.*'s study in [18], where authors obtained least amount of type II error with small loss of plant pixel. However here we have shown that the segmentation in HSV colour space gives better results in more variety of illumination conditions and different species of plants.

4. Conclusions

In this paper we have presented a method for dynamically selecting the suitability of a feature space (colour space in this case) for segmenting plant pixel in a digital image of a plant which has both classes of plant pixels and background pixels modelled in a Gaussian mixture model (GMMs). For the given data set where plants have been imaged under controlled lighting conditions, the proposed method of colour space selection seems to be more effective than the variance ratio method. The HSV colour space clearly performs better for tobacco plants and one of the high quality segmentation performers for Arabidopsis plant images under two different scenarios. Extend this method to plants imaged either in field-like conditions where no lighting control is possible, or close to field-like conditions where there is a mix of ambient and controlled lighting. We can use different distance functions on Gaussian distributions and hence onf $GMMs$ to support the observation with better analytical understanding of the results.

Acknowledgments: The authors are grateful for the financial support from the Australian Research Council through its Linkage program project grants LP140100347.

Author Contributions: P.K. and S.J.M. conceived the experiments; P.K. designed and performed the experiments, and analyzed the data; S.J.M. contributed with funding, computational resources and project management.

Conflicts of Interest: The authors declare no conflicts of interest.

References

1. An, N.; Welch, S.M.; Markelz, R.C.; Baker, R.L.; Palmer, C.M.; Ta, J.; Maloof, J.N.; Weinig, C. Quantifying time-series of leaf morphology using 2D and 3D photogrammetry methods for high-throughput plant phenotyping. *Computers and Electronics in Agriculture* **2017**, *135*, 222 – 232.
2. An, N.; Palmer, C.M.; Baker, R.L.; Markelz, R.C.; Ta, J.; Covington, M.F.; Maloof, J.N.; Welch, S.M.; Weinig, C. Plant high-throughput phenotyping using photogrammetry and imaging techniques to measure leaf length and rosette area. *Computers and Electronics in Agriculture* **2016**, *127*, 376 – 394.
3. Kovalchuk, N.; Laga, H.; Cai, J.; Kumar, P.; Parent, B.; Lu, Z.; Miklavcic, S.J.; Haefele, S.M. Phenotyping of plants in competitive but controlled environments: a study of drought response in transgenic wheat. *Functional Plant Biology* **2016**, *44*, 290–301.
4. Kumar, P.; Cai, J.; Miklavcic, S. High-throughput 3D modelling of plants for phenotypic analysis. Proceedings of the 27th Conference on Image and Vision Computing New Zealand. ACM, 2012, pp. 301–306.

5. Kumar, P.; Connor, J.; Miklavcic, S.J. High-Throughput 3D Reconstruction of Plant Shoots for Phenotyping. Automation Robotics and Computer Vision (ICARCV), 2014 13th International Conference on. IEEE, 2014.
6. Comaniciu, D.; Meer, P. Mean Shift: A Robust Approach Toward Feature Space Analysis. *IEEE Transactions on Pattern Analysis and Machine Intelligence* **2002**, *24*, 603–619.
7. Golzarian, M.R.; Cai, J.; Fric, R.A.; Miklavcic, S.J. Segmentation of Cereal Plant Images Using Level Set Methods – A Comparative Study. *International Journal of Information and Electronics Engineering* **2011**, *1*, 72–78.
8. Valliammal, N.; Geethalakshmi, S.N. Article: A Novel Approach for Plant Leaf Image Segmentation using Fuzzy Clustering. *International Journal of Computer Applications* **2012**, *44*, 10–20. Published by Foundation of Computer Science, New York, USA.
9. Phung, S.L.; Bouzerdoum, A.; Chai, D. Skin Segmentation Using Color Pixel Classification: Analysis and Comparison. *IEEE Trans. Pattern Anal. Mach. Intell.* **2005**, *27*, 148–154.
10. Jones, M.J.; Rehg, J.M. Rehag, "Statistical color models with application to skin detection," Intl. *Journal of Computer Vision* **2002**, pp. 81–96.
11. Vezhnevets, V.; Sazonov, V.; Andreeva, A. A Survey on Pixel-Based Skin Color Detection Techniques. IN PROC. GRAPHICON-2003, 2003, pp. 85–92.
12. Prati, A.; Mikić, I.; Trivedi, M.M.; Cucchiara, R. Detecting moving shadows: Formulation, algorithms and evaluation. *IEEE Transactions on Pattern Analysis and Machine Intelligence* **2003**, *25*, 2003.
13. Fleyeh, H. Color detection and segmentation for road and traffic signs. 2004, Vol. 2, pp. 809–814.
14. Kumar, P.; Sengupta, K.; Lee, A. A comparative study of different color spaces for foreground and shadow detection for traffic monitoring system. Intelligent Transportation Systems, 2002. Proceedings. The IEEE 5th International Conference on. IEEE, 2002, pp. 100–105.
15. Khattab, D.; Ebied, H.M.; Hussein, A.S.; Tolba, M.F. Color Image Segmentation Based on Different Color Space Models Using Automatic GrabCut. *The Scientific World Journal* **2014**, *127*, 1 – 10.
16. Wang, X.; Hansch, R.; Ma, L.; Hellwich, O. Comparison of Different Color Spaces for Image Segmentation using Graph-cut. Proceedings of the International Conference on Computer Vision Theory and Applications (VISAPP), 2014, pp. 301–308.
17. Muselet, D.; Macaire, L. Combining color and spatial information for object recognition across illumination changes. *Pattern Recognition Letters* **2007**, *28*, 1176 – 1185.
18. Golzarian, M.R.; Lee, M.K.; Desbiolles, J.M.A. Evaluation of Color Indices for Improved Segmentation of Plant Images. *Transactions of the ASABE* **2012**, *55*, 261–273.
19. Levina, E.; Bickel, P. The Earth Mover's distance is the Mallows distance: Some insights from statistics. Proceedings of the IEEE International Conference on Computer Vision, 2001, Vol. 2, pp. 251 – 256.
20. Zhao, Q.; Brennan, S.; Tao, H. Differential EMD Tracking. Proceedings of the IEEE International Conference on Computer Vision, 2007, pp. 1–8.
21. Kumar, P.; Dick, A. Adaptive earth movers distance-based Bayesian multi-target tracking. *Computer Vision, IET* **2013**, *7*, 246–257.
22. Wyszecki, G.; Stiles, W.S. *Color Science: Concepts and Methods, Quantitative Data and Formulae*; Wiley, 2000; chapter 6.
23. Busin, L.; Vandenbroucke, N.; Macaire, L. Color Spaces and Image Segmentation; Elsevier, 2009; Vol. 151, *Advances in Imaging and Electron Physics*, pp. 65 – 168.
24. Rubner, Y.; Tomasi, C.; Guibas, L.J. The earth mover's distance as a metric for image retrieval. *International Journal of Computer Vision* **2000**, *40*, 99–121.
25. Hitchcock, F.L. The distribution of a product from several sources to numerous localities. *Journal of Math. Phys.* **1941**, *20*, 224–230.
26. Rubner, Y.; Tomasi, C.; Guibas, L.J. A metric for distributions with applications to image databases. Sixth International Conference on Computer Vision (IEEE Cat. No.98CH36271), 1998, pp. 59–66.
27. Shirdhonkar, S.; Jacobs, D. Approximate earth mover's distance in linear time. Computer Vision and Pattern Recognition, 2008, pp. 1 –8.
28. Ling, H.; Okada, K. An Efficient Earth Mover's Distance Algorithm for Robust Histogram Comparison. *IEEE Transactions on Pattern Analysis and Machine Intelligence* **2007**, *29*, 840–853.
29. Mahalanobis, P.C. On the generalised distance in statistics. *Proceedings of the National Institute of Sciences of India* **1936**, *2*, 49–55.

30. Liu, Y.; Schmidt, K.L.; Cohn, J.F.; Mitra, S. Facial asymmetry quantification for expression invariant human identification. *Computer Vision and Image Understanding* **2003**, *91*, 138 – 159. Special Issue on Face Recognition.
31. Liu, Y.; Teverovskiy, L.; Carmichael, O.; Kikinis, R.; Shenton, M.; Carter, C.; Stenger, V.; Davis, S.; Aizenstein, H.; Becker, J.; Lopez, O.; Meltzer, C. Discriminative MR Image Feature Analysis for Automatic Schizophrenia and Alzheimer's Disease Classification. In *Medical Image Computing and Computer-Assisted Intervention – MICCAI 2004*; Barillot, C.; Haynor, D.; Hellier, P., Eds.; Springer Berlin Heidelberg, 2004; Vol. 3216, *Lecture Notes in Computer Science*, pp. 393–401.
32. Collins, R.T.; Liu, Y.; Leordeanu, M. Online Selection of Discriminative Tracking Features. *IEEE Transactions on Pattern Analysis and Machine Intelligence* **2005**, *27*, 1631–1643.